npj computational materials

www.nature.com/npjcompumats

ARTICLE OPEN

Check for updates

How coherence is governing diffuson heat transfer in amorphous solids

Zhongwei Zhang[1]✉, Yangyu Guo[1], Marc Bescond[2,3], Jie Chen[4]✉, Masahiro Nomura[1] and Sebastian Volz[1,2,4]✉

Thermal transport in amorphous materials has remained one of the fundamental questions in solid state physics while involving a very large field of applications. Using a heat conduction theory incorporating coherence, we demonstrate that the strong phase correlation between local and non-propagating modes, commonly named diffusons in the terminology of amorphous systems, triggers the conduction of heat. By treating the thermal vibrations as collective excitations, the significant contribution of diffusons, predominantly relying on coherence, further reveals interesting temperature and length dependences of thermal conductivity. The propagation length of diffuson clusters is found to reach the micron, overpassing the one of propagons. The explored wavelike behavior of diffusons uncovers the unsolved physical picture of mode correlation in prevailing models and further provides an interpretation of their ability to transport heat. This work introduces a framework for understanding thermal vibrations and transport in amorphous materials, as well as an unexpected insight into the wave nature of thermal vibrations.

npj Computational Materials (2022)8:96 ; https://doi.org/10.1038/s41524-022-00776-w

INTRODUCTION

Heat conduction in different states of matter exhibits diverse characteristics along with different modalities of lattice vibration, whereas driving performances in several devices and materials related fields impacted by thermal management or energy conversion. While an adequate understanding of phonons in crystals is well established, a debate still exists regarding the physical pictures of thermal vibrations and transport in amorphous materials[1–6]. Owing to the loss of the long-range lattice periodicity, the concept of phonons becomes invalid in amorphous materials and the application of the phonon-gas model for thermal transport is accordingly failing[7–11]. The limited comprehension of thermal vibrations in amorphous materials has hindered their advanced applications. In the past decades, diverse attempts have proposed theoretical frames to describe thermal vibrations and transport in amorphous materials[7–9,12–15]. Particularly, Allen and Feldman[7,8,16] established a classification of lattice vibrations into propagons, diffusons and locons. Propagons correspond to low-frequency propagating waves and locons to high-frequency localized states, while diffusons designate local modes characterized by intermediate frequencies. Their further studies demonstrated that the off-diagonal terms of the group velocity operator plays a critical role in the transport of diffusons[8,9,17]. In a recent work, Isaeva et al.[13] developed a quasi-harmonic Green-Kubo (QHGK) model to study the thermal transport in amorphous materials by including a scattering correlation between different modes. The Allen-Feldman and QHGK models share the common conceptual basis of mode correlation.

On the other hand, the study of the physical picture of thermal vibrations in amorphous materials has also attracted significant attention. In both Allen-Feldman and QHGK models, thermal vibrations are treated as plane waves in which the normal modes and scatterings are obtained from the harmonic and anharmonic lattice dynamic approaches, respectively[9,13,16]. The utilized normal modes and ill-defined group velocity[10] raise questions on the fundamentals of Allen-Feldman and QHGK descriptions.

In addition, in analogy to liquids, the collective excitations are experimentally observed and proposed to understand thermal vibrations, in analogy to liquids[18–23]. Moon et al.[20,21] found that the thermal transport in amorphous silicon (a-Si) is dominated by acoustic collective excitations rather than by normal modes and that the elastic scattering predominates. The obtained variation of lifetimes is well consistent with the frequency of the boson peak and the Ioffe-Regel crossover[18,21]. A theoretical model that can assess the thermal transport in amorphous materials by directly incorporating the collective excitations, however, is still missing. In addition, the controversies regarding the dependences of thermal conductivity (κ) on temperature and length remain topics of debate[23–27].

In this work, we theoretically investigate thermal transport in amorphous silicon, in which thermal vibrations are simultaneously interpreted as the composition of particlelike and wavelike components. The strong phase correlation or in other terms, the coherence between several diffusons, is firstly studied from wave-packet simulations and the behaviors of propagons and diffusons are clearly discriminated. Then, we apply our recently developed coherence heat conduction model[28] by estimating mode lifetimes and coherence times. The significant contribution of phase correlation to thermal conductivity is uncovered. The estimated propagation length of coherent diffusons is found beyond the one of propagons. We finally demonstrate a fundamental, unforeseen and accurate point of view to understand thermal vibrations and transport in amorphous materials.

[1]Institute of Industrial Science, The University of Tokyo, Tokyo 153-8505, Japan. [2]Laboratory for Integrated Micro and Mechatronic Systems, CNRS-IIS UMI 2820, The University of Tokyo, Tokyo 153-8505, Japan. [3]IM2NP, UMR CNRS 7334, Aix-Marseille Université, Faculté des Sciences de Saint Jérôme, Case 142, 13397 Marseille Cedex 20, France. [4]Center for Phononics and Thermal Energy Science, School of Physics Science and Engineering and China-EU Joint Lab for Nanophononics, Tongji University, 200092 Shanghai, People's Republic of China. ✉email: zhongwei@iis.u-tokyo.ac.jp; jie@tongji.edu.cn; volz@iis.u-tokyo.ac.jp

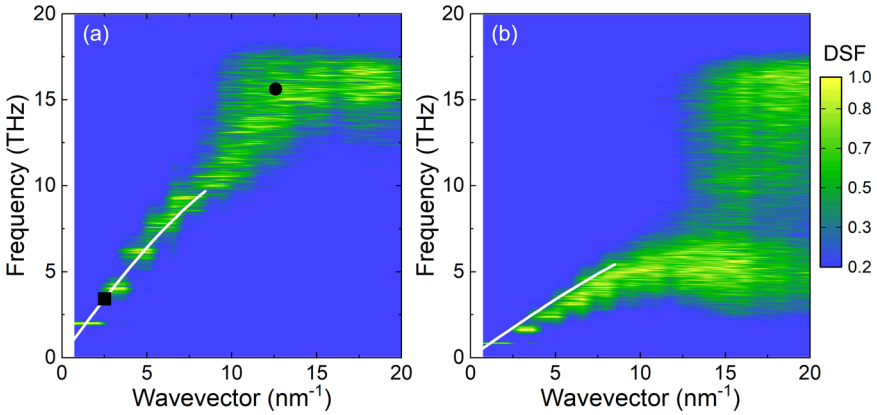

Fig. 1 Dynamical structure factor. The calculated dynamical structure factor (DSF) of amorphous silicon for the longitudinal (**a**) and transverse (**b**) excitations at room-temperature. The calculated amorphous silicon contains 4096 atoms. The solid white lines are, respectively, the phonon dispersion of the longitudinal branch (**a**) and the transverse branch (**b**) for crystal silicon. The dots in (**a**) are the specific vibrations that applied in wave-packet simulations.

RESULTS AND DISCUSSION

Dynamical structure factor

Considering the atomic instability and the absence of lattice periodicity in amorphous materials, thermal vibrations in a-Si are treated as collective excitations as studied from the dynamical structure factor (DSF)[21,23]. Those excitations also refer to acoustic collective excitations, where atoms are vibrating along the same polarization (See Supplementary Equations (1) and (2)). The concept of collective excitation was initially implemented to describe liquids or liquid-like matters[29]. The similarity in the lattice aperiodicity and atomic instability makes the collective excitation a reasonable description of thermal vibrations in amorphous materials as discussed before in refs. [21,23,30]. The calculated DSF is shown in Fig. 1, which includes the longitudinal and transverse polarizations (See calculation details in Supplementary Methods). The widening of the wavevector in Fig. 1 is inversely proportional to the system size. In this work, we employ an amorphous system of 4096 atoms, which is large enough to accurately capture the vibrational properties and suppress the size effect according to ref. [27].

Similarly to the behavior of phonons in crystals, the longitudinal and transverse polarizations show distinct tendencies due to a lower group velocity of the collective transverse mode. In addition, the results in Fig. 1 show that the dispersion of collective excitations in the small wavevector region agrees well with the acoustic branches of silicon crystal (white lines), indicating that the collective excitations can highly inherit thermal vibrations from the corresponding crystal. Moreover, an obvious increase in the broadening of polarizations after ~10 nm^{-1} is also observed. The threshold wavevector of this broadening corresponds to the first Brillouin zone boundary of the crystal and the transition from propagons to diffusons (See Fig. 1). Figure 1 also indicates that the longitudinal and transverse polarizations have different transition frequencies. Note that the transition frequency of the transverse polarization is directly linked to the frequency of the boson peak[18]. As demonstrated before[21], the broadening is inversely related to the modal lifetime. The transition from propagons to diffusons appears as a significant change of lifetimes, which will be highlighted in the afterward discussion.

Wave-packet simulation

In contrast to the estimation of the frequencies of the lattice vibrations obtained from the normal mode analysis, which is only carried out at the Gamma point, the DSF in Fig. 1 can also provide the information of wavevector for different vibrations but in the frame of collective excitations as proposed in refs. [21,23,30]. By implementing the wave-packet simulation, we further study the detailed transport properties of propagons and diffusons. The approach to excite wave-packets is presented in Methods, where the environment temperature is set to 0.01 K to avoid inelastic/anharmonic scattering. To excite different states in a-Si, the wavevectors for longitudinal propagons and diffusons are, respectively, chosen as 2.5 and 12.5 nm^{-1} as marked by the dots in Fig. 1(a). Figure 2(a) depicts the schematic figure of a wave-packet simulation and its propagation, in which the excited wave-packet is propagating along the *x* direction in a-Si. In each interval of 0.05 ps, the energy of this propagating wave-packet is recorded and the spatial wavelet transform is performed to calculate the variation of the coherence length (l_c) of this wave-packet (See Supplementary Methods). Figure 2(b), (c), respectively, show the variation of energy and l_c of propagons and diffusons. The energies of these two types of vibrations gradually decay during their propagation. As the environment temperature is low enough to weaken the anharmonic scattering, the energy decrease in Fig. 2(b), (c) indicates the significance of elastic scattering in the dissipation of thermal vibrations in amorphous materials. In addition, the energy of diffusons decays much faster than that of propagons indicating a stronger elastic scattering for the non-propagating diffusons, which agrees well with previous predictions[21,23].

On the other hand, a unique effect of elastic scattering on coherence is observed. Figure 2(b), (c) show that the coherence length l_c decreases significantly slower than the energy. The difference indicates that during elastic scattering, the vibrational amplitude of wave-packets decreases, resulting in the dissipation of energy. Simultaneously, the spatial extension of wave-packets remains constant with high coherence until full disappearance (See the schematic in Fig. 2(a)). The zeroed coherence length l_c corresponds to the extinction of wave-packets excitation, as a result of elastic scattering. To model the realistic system that contains a high density of wave-packets in the same mode, the systems with 50 and 150 wave-packets are also studied. Compared to the limited effect on energy decrease due to the predominant elastic scattering, a stronger effect on l_c is found. For propagons, l_c decreases with the increase of the wave-packets number, which might be originated from the anharmonic interaction between wave-packets, as the environment energy or temperature is increasing with the wave-packet number. On the contrary, the decay of diffusons l_c is reversely delayed, which should result from the wavelike interaction between diffusons or equivalently from phase correlation instead of anharmonicity. The difference also results in a faster extinction of propagons wave-packets as the number of wave-packets increases to 150 WPs.

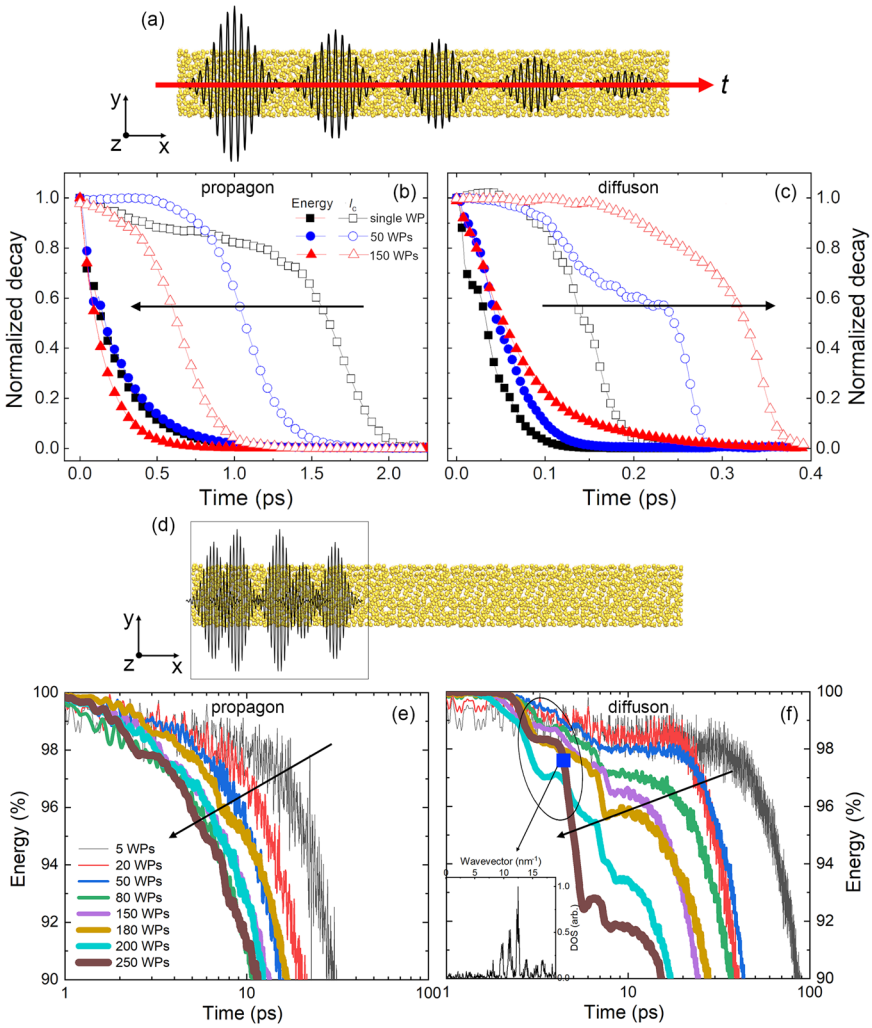

Fig. 2 Wave-packets simulation. a Schematic figure of wave-packets propagating in amorphous silicon. **b** Normalized decay trends of energy and coherence length (l_c) versus simulation time in the cases of single-propagon wave-packet (WP), of 50 and of 150 wave-packets (WPs). **c** Normalized decay trends of energy and coherence length (l_c) versus simulation time in the cases of a single-diffuson WP, of 50 and of 150 diffuson WPs. The arrows indicate the shift of l_c with increasing wave-packets number. **d** Schematic of wave-packet excitations in amorphous silicon. The black box indicates the initial excited region with a length of 30 nm and the corresponding energy is recorded. Energy percentage versus simulation time for the different numbers of (**e**) propagon wave-packets and (**f**) diffuson wave-packets. The arrows indicate the shift of energy decrease with increasing wave-packets number. The inset in (**f**) shows the density of states (DOS) at 4 ps in the 250 wave-packets case.

The phase correlation between different wave-packets of diffusons should be understood as mutual coherence[31], which is different from the intrinsic coherence appearing in phononic or simple crystals[32]. The weak mutual coherence in Fig. 2(a) indicates that the coherence behavior of propagons here is similar to the one of phonons in simple crystals. The strong coherence of diffusons manifested by this unconverged increase of l_c should greatly influence the thermal energy decay and transport in a realistic system having a high density of wave-packets.

The influence of coherence on thermal transport is further investigated from the wave-packet simulations in Fig. 2(d–f). In this simulation, several wave-packets are randomly excited in a well-defined region of length 20 nm and then the energy within this region is recorded (See the box in Fig. 2(d)). As increasing the number of wave-packets, the recorded energy change correspondingly increases. At low density, diffusons show low thermal transport efficiency in Fig. 2(f). However, as the wave-packet number reaches 50, a sudden energy change appears around 4 ps, indicating a high transport efficiency, which becomes more pronounced as up to 250 wave-packets. The additional density of states calculation in the inset of Fig. 2(f) indicates that the system of 250 wave-packets at 4 ps is still dominated by diffusons with wavevector higher than 10 nm^{-1} and the enhanced transport efficiency is still related to the behavior of diffusons. On the contrary, the transport efficiency of propagons in Fig. 2(e) follows a monotonic decreasing trend with simulation time.

To further evaluate the coherence effect on thermal transport efficiency, the spatial heat flux distribution is calculated in Fig. 3. The heat flux is obtained at the time of the enhanced energy change appearing ~4 ps. For the systems with a small number of wave-packets in Fig. 3(a), (c), the less-propagating and low-density diffusons generate a lower heat flux than in the case of propagons. While increasing the number of wave-packets to 250 in Fig. 3(b), (d), diffusons reversely carry a more significant heat flux than propagons. On the other hand, compared to the dense oscillations at low density, the heat flux of diffusons at high density exhibits more unified oscillations, indicating the generation of in-phase/coherent propagating waves due to the strong phase correlation. The strong phase correlation and high heat flux for the case of 250 wave-packets are the cause to the pronounced increase of thermal transport efficiency in Fig. 2(f), even compared to the case of 200 wave-packets. Note that the phase correlation

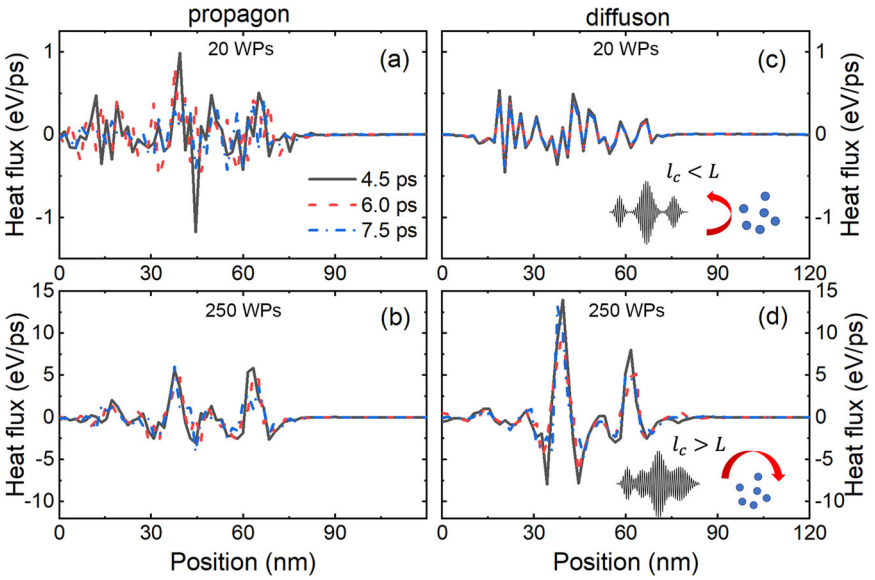

Fig. 3 Heat flux distribution. The simulated heat flux for the cases where propagons are excited with (**a**) 20 wave-packets and (**b**) 250 wave-packets at 4 ps. The simulated heat flux for the cases where diffusons are excited with (**c**) 20 wave-packets and (**d**) 250 wave-packets at 4 ps. The inset of figure (**c**) shows the schematic of a low-density ensemble of wave-packets reflected by the local disorder. The inset of (**d**) shows the schematic of a high-density ensemble of coherent diffuson wave-packets propagating through the local disorder.

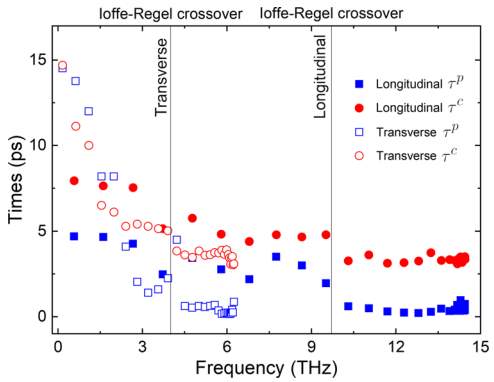

Fig. 4 Calculated lifetime (τ^p) and coherence time (τ^c) of amorphous silicon at room-temperature. The vertical lines indicate the Ioffe-Regel crossover for the longitudinal and transverse polarizations.

between diffusons might be related to the reported spatial correlations of local stress[33]. As displayed in the inset of Fig. 3(c) and 3(d), the less-propagating nature and low density of diffusons lead to a state of quasi-localization with low thermal transport efficiency, in which the coherence length is smaller than the length-scale of local disorder (L), $l_c < L$. However, the high density results for diffusons seem to refer more to coherent wave-packets that are phase correlated, yielding a high thermal transport efficiency. In a realistic system, vibrations are randomly and extensively excited by thermal energy in analogy to the simulated cases with large density wave-packets (See Figs. 2(c) and 3(d)). This high transport efficiency here agrees well with the previously reported high diffuson contribution to thermal conductivity[10,34,35]. The study in Fig. 3 eventually reports the unexpected effect and physical picture of coherence on the transport of diffusons in amorphous materials.

Lifetime and coherence time

With the coherence calculation in Supplementary Methods[28,31], we estimated the lifetimes and coherence times for different collective excitation modes in Fig. 4. Similarly to the frequency dependence in crystal, the lifetimes and coherence times of a-Si decrease with frequency in the low-frequency region. Beyond several Terahertz, the lifetimes of both transverse and longitudinal polarizations approache to zero. This trend corresponds to the one predicted by the Ioffe-Regel crossover as indicated by the vertical reference lines in Fig. 4. Obviously, the Ioffe-Regel crossover is polarization dependent and the transverse polarization is characterized by a lower frequency of Ioffe-Regel crossover. After the Ioffe-Regel crossover, thermal vibrations in a-Si shift to the diffuson region. The previous classification of propagons and diffusons from the normal mode analysis is probably insufficient, as the polarizations are not properly distinguished[8,36–38].

On the other hand, the coherence time displays different dependences on frequency. For low-frequency vibrations, or propagons, the coherence times also decrease with the frequency and the values of coherence time are close to that of lifetimes. At high frequencies, diffusons have longer coherence times than lifetimes and quickly converge. The pronounced coherence time agrees well with our previous discussion about the strong phase correlation between diffuson modes.

Coherent thermal transport

The significant impact of the wavelike behavior on the transport and dynamics has been widely observed in phononic crystals and low-dimensional materials[39–42]. In our recent work, by introducing the coherence related to the temporal extension of wave-packets, the coherence effect on the mode dynamics is studied with Supplementary Equation 14.[28,31] Correspondingly, the complete thermal conductivity (κ_{p+w}) including both the particlelike (p) and wavelike (w) behaviors can be expressed as[28,31]

$$\kappa_{p+w} = \frac{1}{3}\sum_{\alpha}\sum_{v} C_{v,v}^{\mathrm{clas}} v_{v,\alpha}^2 \sqrt{\frac{\pi}{4\ln 2}}\tau_v^c e^{\frac{\tau_v^{c2}}{128\ln 2\tau_v^{p2}}}. \quad (1)$$

Here, $v_{v,\alpha}$ denotes the group velocity of mode v along the cartesian coordinate α. $C_{v,v}^{\mathrm{clas}} = k_B/V$ is the classical specific heat per mode. The modal coherence time and lifetime are obtained from previous coherence calculations[28,31] reported in Fig. 4. The particlelike thermal conductivity can be calculated with the Peierls-Boltzmann formula[43] as $\kappa_p = \frac{1}{3}\sum_{\alpha}\sum_{\lambda} C_{v,v}^{\mathrm{clas}} v_{v,\alpha}^2 \tau_v^p$.

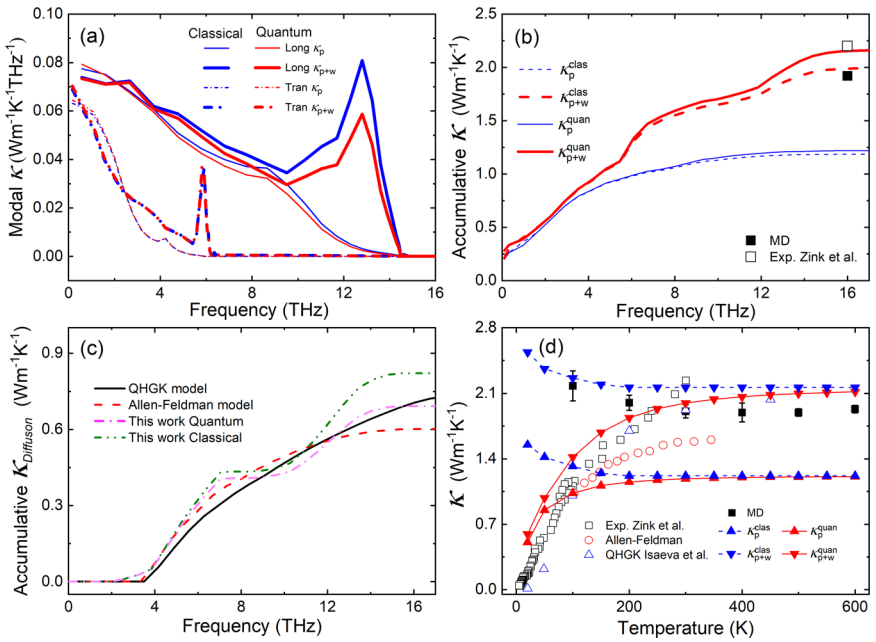

Fig. 5 The thermal conductivity of amorphous silicon. a Modal classical and quantum thermal conductivities (κ) of amorphous silicon for the longitudinal (Long) and transverse (Tran) polarizations, respectively, from the particlelike (κ_p) and overall (particlelike + wavelike (κ_{p+w})) contributions at 300 K. **b** Accumulative thermal conductivities versus frequency at 300 K. **c** Accumulative thermal conductivities of diffusons versus frequency from the quasi-harmonic Green-Kubo (QHGK) model, the Allen-Feldman model and this work at 300 K. **d** Thermal conductivities versus temperature. The symbols refer to experimental results (Exp.)[44], QHGK model, Allen-Feldman model and our molecular dynamic (MD) simulations, see calculation details in Supplementary Methods.

Obviously, the calculation of thermal conductivity from Eq. (1) depends on frequency, group velocity, lifetime and coherence time. In contrast to the ill-defined normal mode analysis, these quantities can be obtained from the collective excitation picture provided by the DSF spectrum showing sufficiently clear dispersion as proposed by Moon et al.[20,21]. Especially, the group velocity can be calculated according to $\boldsymbol{u}_v = d\omega_v/d\boldsymbol{q}$. The relationship between ω_v and $\boldsymbol{q}$ is determined by the DSF spectrum for the transverse and longitudinal polarizations. The details of the determination of the frequency for different wavevectors and polarizations are presented in Supplementary Discussion. The frequency and group velocity have been illustrated in Supplementary Figure 3. Our wave-packet simulations also indicate that the predominant vibrations in amorphous materials manifest a strong wavelike behavior, which can be captured by Eq. (1) via the coherence time. The estimations can be further quantum corrected by replacing $C_{v,v}^{clas}$ by the quantum specific heat $C_{v,v}^{qua}$, here $C_{v,v}^{qua} = \frac{k_B exp(x)}{V}\left[\frac{x}{exp(x)-1}\right]^2$ with $x = \frac{\hbar\omega_v}{k_B T}$. Obviously, the calculation of thermal conductivity in Eq. (1) is only based on the information extracted from the DSF spectrum and wavelet transform. We thus believe that the following demonstrations can also be generalized to other amorphous solids, for instance, amorphous SiO_2 and amorphous SiN.

Figure 5 reports the thermal conductivities calculated from different approaches. In Fig. 5(a), the particlelike contribution to thermal conductivity, κ_p, exhibits the same tendency as the predictions in crystals, where κ_p decreases with the frequency in the low-frequency region. However, the particlelike contributed thermal conductivity is lower than the one from experimental measurements[44] and direct MD Green-Kubo prediction (See the accumulative κ in Fig. 5(b) and the Green-Kubo calculation in Supplementary Methods). The modal contribution indicates that by only considering the particlelike behavior of thermal vibrations, the contribution from diffusons at high frequencies cannot be captured (thinner lines). This outcome also manifests that the dynamics of diffusons is mainly dominated by the wavelike behavior, which is consistent with the results of the wave-packet simulations. On the other hand, the coherence has negligible contribution to thermal transport for low-frequency propagons, as the values of lifetimes are close to that of coherence times in Fig. 4. This negligible contribution of coherence indicates that the behavior of propagons is similar to the one of room-temperature normal phonons in simple crystals, in which the mutual coherence between propagons is too weak to influence the thermal transport[31].

We further investigate the coherence corrected thermal conductivity from Eq. (1) in Fig. 5. Compared to the weak wavelike contribution from low-frequency propagons, the wavelike thermal conductivity predominates the heat conduction of high-frequency diffusons (thicker lines in Fig. 5(a)), indicating the strong phase correlation effect on diffusons and its significant contribution to thermal transport. The peaks of modal thermal conductivity in Fig. 5(a) are corresponding to the high contribution from transverse and longitudinal diffusons to thermal conductivity. The large wavelike contribution from diffusons to thermal conductivity well coincides with the enhanced propagating efficiency in wave-packet simulations described above. The accumulative thermal conductivity of a-Si in Fig. 5(b) shows that the coherence corrected room-temperature thermal conductivity agrees well with the experimentally measured value and the MD Green-Kubo κ. The correction degree, $\frac{\kappa_{p+w}-\kappa_p}{\kappa_p} \times 100\%$, reaches 68 % under the quantum approximation and the contribution is mainly arising from frequencies larger than 4 THz. In addition, due to the high-frequency range of diffusons, the quantum effect on the propagon population only quantitatively influences the thermal conductivity values.

Compared to the prevailing models, we provide a physical understanding of diffuson propagation arising from the strong phase correlation. The comparison between different theories yielding the estimation of the thermal conductivity from diffusons, $\kappa_{Diffuson}$, is further presented in Fig. 5(c). The contribution from diffusons is accumulated from modes with frequencies larger than

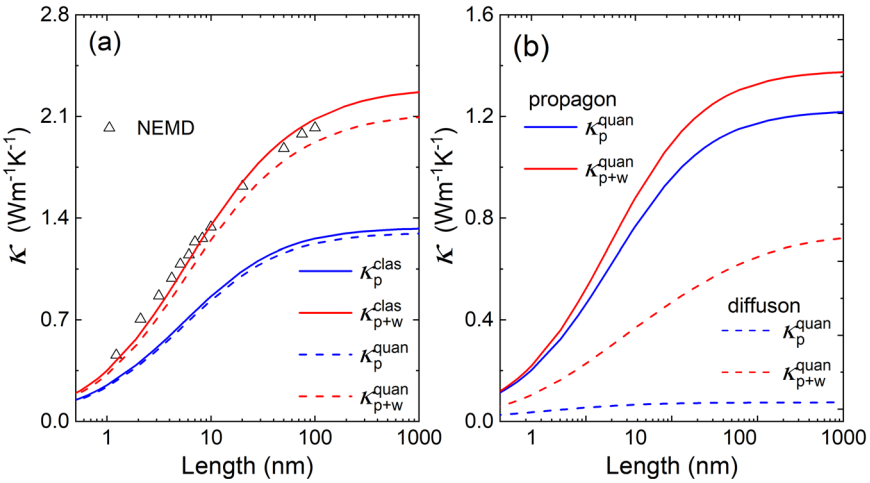

Fig. 6 Length-dependent thermal conductivity of amorphous silicon at 300 K. a Length-dependent classical and quantum thermal conductivity of amorphous silicon, respectively, from particlelike and wavelike contributions at 300 K. The symbols denote the results from non-equilibrium molecular dynamic (NEMD) simulations. **b** Length-dependent quantum thermal conductivity, respectively, from propagons and diffusons at 300 K.

the Ioffe-Regel crossover. Three different models correct the thermal conductivity due to the following effects, (i) in our model, the phase correlation/coherence between diffusons; (ii) in the QHGK model, the correlation between different modal scatterings, i.e., off-diagonal scattering terms; (iii) in the Allen-Feldman model, the off-diagonal terms of the group velocity operator. Figure 5(c) shows that our prediction is in excellent agreement with the results from both the Allen-Feldman and QHGK models in a wide frequency region. The higher values obtained at the classical limit are due to the overestimation of the phonon population at high frequencies. The plateau between 7 and 10 THz in Fig. 5(c) is originated from the different dominant frequency ranges for transverse and longitudinal diffusons (See Fig. 5(a)). The results of Allen-Feldman and QHGK models are, respectively, calculated from the packages of GULP[45] and κALDo[46] with the same a-Si configuration as implemented in the DSF calculations.

The comparison between the temperature dependent thermal conductivities is displayed in Fig. 5(d). Our predicted quantum thermal conductivities, κ_{p+w}^{quan}, agree satisfactorily with the predictions from other theoretical models and experimental values in the full temperature regime, confirming also a higher accuracy compared to the estimations from the Allen-Feldman model. Compared to the high thermal conductivities acquired from direct MD simulations in the classical limit, the quantum effects can be effectively treated resulting in a thermal conductivity decrease when temperature decreases. In addition, the fast convergence of thermal conductivity and the negligible temperature dependence at high temperatures indicate weakly anharmonic scattering processes and the predominant elastic scattering in a-Si. Figure 5 (d) also shows that the coherence correction to the thermal conductivity becomes more pronounced as temperature increases, manifesting the enhanced phase correlation between modes with temperature as demonstrated recently in complex crystals[12]. Moreover, considering the broad application of composite materials[47], the variation of coherence across the interfaces between amorphous and crystals should be an important topic worth to explore in the future.

Length dependence

The obtained vibrational properties from DSF calculations are analogous to the phononic properties of a crystal. In principle, the diverse scatterings can be incorporated into the Matthiesse's law

$$\frac{1}{\tau_\nu^{tot}} = \frac{1}{\tau_\nu^{d}} + \frac{1}{\tau_\nu^{b}}, \tag{2}$$

where, τ_ν^{d} refers to the decay time $\sqrt{\frac{\pi}{4\ln 2}}\tau_\nu^{p} e^{\frac{\tau_\nu^{c2}}{128\ln 2\,\tau_\nu^{p2}}}$ in Eq. (1) due to the anharmonic and elastic scatterings in Eq. (S14). The boundary scattering time τ_ν^{b} is calculated as $\tau_\nu^{b} = \frac{2L_s}{|v_\nu|}$[48], where L_s is the length of the system. As a comparison, the length-dependent thermal conductivity is also calculated from non-equilibrium molecular dynamic (NEMD) simulations in Fig. 6(a) by following our previous procedure used in crystalline nanostructures[49].

Figure 6 (a) shows that the coherence corrected thermal conductivities are in fair agreement with NEMD predictions. The limited discrepancies might be originating from the uncertainty of NEMD simulations. The purely particlelike contribution underestimates the thermal energy carriers with long propagation lengths. Recent measurements revealed that the thermal conductivity of a-Si displays a marked length dependence and the ultra-long mean free paths can reach several hundreds of nanometers[23,50–52]. Our predictions in Fig. 6(a) indicate that this long length dependence might result from the contribution of coherent diffusons. On the other hand, the agreement between the predictions from our model and NEMD simulations demonstrates the validation of treating the vibrations in amorphous materials as collective excitations that have specific polarizations and group velocities.

We further quantify the length-dependent contributions of propagons and diffusons by following the Ioffe-Regel crossover. As shown in Fig. 6(b), the coherence has a limited effect on the propagon thermal conductivity. As discussed in our previous work, the small size and highly propagative wave-packets of thermal vibrations should exhibit weak intrinsic coherence[31], which is the case of propagons in a-Si. However, diffusons are non-propagative and localized lattice waves, which makes them more correlated and thus exhibiting a stronger coherence. Correspondingly, their wavelike behavior results in long propagation lengths and a high diffuson thermal conductivity.

In this work, we demonstrated the strong phase correlation of diffusons in amorphous silicon. Wave-packet simulations show that due to their localized nature and wavelike behavior, diffusons can be highly correlated and exhibit high transport efficiency. The presence of collective excitations and the predominance of elastic

scattering are also demonstrated. The agreements between a heat conduction model including coherence effects and other results from prevailing theories not only validate the generalization of our model to different systems but also show the unexpected and significant coherence effect on the thermal conductivity of amorphous materials. The past discrepancies and recent measurements of the temperature and length dependences of thermal conductivity are well explained by the exploration of the phase correlation between diffusons. This work provides a framework to understand the thermal vibrations and transport in amorphous materials, it will finally help predict and analyze the behavior of disordered solids in general.

METHODS

Molecular dynamic simulations

All molecular dynamic (MD) simulations are carried out using the LAMMPS package[53] with a time step of 0.35 fs. The Si–Si interactions in silicon systems are modeled by the Stillinger-Weber potential[54]. a-Si is prepared from a melt-quench procedure. The details about this procedure can be found in ref. [55]. The further calculation of the radial distribution function indicates that the obtained amorphous silicon model has been fully amorphized after the melt-quench procedure (see details in Supplementary Discussion). In this work, the a-Si system contains 4096 atoms and is studied in the equilibrium molecular dynamic (EMD) simulations with periodic boundary conditions in all directions. After the structure relaxation and thermal equilibration in the isothermal-isobaric (NPT) ensemble for 500 ps, EMD simulations with the microcanonical (NVE) ensemble are performed to record the atomic trajectories.

Wave-packet simulation

The wave-packet simulation applied to study the propagation of propagons and diffusons is implemented by altering the atomic position from the equilibrium state. To ensure enough space and time for the observation of wave-packet propagation along one direction, a $20 \times 1 \times 1$ supercell based on a system that contains 4096 atoms is applied in the wave-packet simulations. The periodic boundary conditions are applied in all directions. Firstly, the structure is relaxed at 0.01 K in the canonical (NVT) ensemble for 300 ps. At such a low temperature, we can ensure that the system is in a weakly anharmonic state and inelastic scattering is not involved. Then, the space dependent atomic displacement (ΔD) of the wave-packet is introduced in the following form[40,56,57]

$$\Delta D(x) = A_0 e^{[i(x-x_0)/\lambda]} e^{\left[-\frac{1}{2}\left(\frac{x-x_0}{\Delta}\right)^2\right]}, \quad (3)$$

where A_0 denotes the amplitude and x_0 the center position of the wave-packet. λ is the wavelength of a specific mode and Δ is the spatial width of the wave-packet. The relationship between wavelength λ and wavevector $\mathbf{q}$ is $\lambda = \frac{2\pi}{|\mathbf{q}|}$. In order to introduce several wave-packets, A_0 and x_0 are randomly set to generate a correspondingly random distribution of wave-packets.

DATA AVAILABILITY

Data available on reasonable request from the authors.

CODE AVAILABILITY

The code providing the temporal coherence time and thermal conductivity computed with coherence effects can be found as an open-source package in https://github.com/ZhongweiZhangsite/WPPT.

Received: 10 November 2021; Accepted: 4 April 2022;
Published online: 29 April 2022

REFERENCES

1. Pohl, R. O., Liu, X. & Thompson, E. Low-temperature thermal conductivity and acoustic attenuation in amorphous solids. *Rev. Mod. Phys.* **74**, 991–1013 (2002).
2. Cahill, D. G. & Pohl, R. O. Thermal conductivity of amorphous solids above the plateau. *Phys. Rev. B* **35**, 4067–4073 (1987).
3. Wingert, M. C., Zheng, J., Kwon, S. & Chen, R. Thermal transport in amorphous materials: a review. *Semicond. Sci. Technol.* **31**, 113003 (2016).
4. DeAngelis, F. et al. Thermal transport in disordered materials. *Nanoscale Microscale Thermophys. Eng.* **23**, 81–116 (2019).
5. Zhou, W.-X. et al. Thermal conductivity of amorphous materials. *Adv. Funct. Mater.* **30**, 1903829 (2020).
6. Zhang, Z. et al. Size-dependent phononic thermal transport in low-dimensional nanomaterials. *Phys. Rep.* **860**, 1–26 (2020).
7. Feldman, J. L., Kluge, M. D., Allen, P. B. & Wooten, F. Thermal conductivity and localization in glasses: numerical study of a model of amorphous silicon. *Phys. Rev. B* **48**, 12589–12602 (1993).
8. Allen, P. B. & Feldman, J. L. Thermal conductivity of disordered harmonic solids. *Phys. Rev. B* **48**, 12581–12588 (1993).
9. Allen, P. B., Feldman, J. L., Fabian, J. & Wooten, F. Diffusons, locons and propagons: character of atomie yibrations in amorphous Si. *Philos. Mag. B* **79**, 1715–1731 (1999).
10. Lv, W. & Henry, A. Examining the validity of the phonon gas model in amorphous materials. *Sci. Rep.* **6**, 37675 (2016).
11. Lv, W. & Henry, A. Non-negligible contributions to thermal conductivity from localized modes in amorphous silicon dioxide. *Sci. Rep.* **6**, 35720 (2016).
12. Simoncelli, M., Marzari, N. & Mauri, F. Unified theory of thermal transport in crystals and glasses. *Nat. Phys.* **15**, 809–813 (2019).
13. Isaeva, L., Barbalinardo, G., Donadio, D. & Baroni, S. Modeling heat transport in crystals and glasses from a unified lattice-dynamical approach. *Nat. Commun.* **10**, 3853 (2019).
14. Xi, Q. et al. Hopping processes explain linear rise in temperature of thermal conductivity in thermoelectric clathrates with off-center guest atoms. *Phys. Rev. B* **96**, 064306 (2017).
15. Xi, Q. et al. Off-center rattling triggers high-temperature thermal transport in thermoelectric clathrates: nonperturbative approach. *Phys. Rev. B* **97**, 2–3 (2018).
16. Bickham, S. Numerical study of low-frequency vibrations in amorphous silicon. *Phys. Rev. B* **59**, 3551–3559 (1999).
17. Hardy, R. J. Energy-flux operator for a lattice. *Phys. Rev.* **132**, 168 (1968).
18. Shintani, H. & Tanaka, H. Universal link between the boson peak and transverse phonons in glass. *Nat. Mater.* **7**, 870–877 (2008).
19. Larkin, J. M. & McGaughey, A. J. Thermal conductivity accumulation in amorphous silica and amorphous silicon. *Phys. Rev. B* **89**, 144303 (2014).
20. Moon, J., Latour, B. & Minnich, A. J. Propagating elastic vibrations dominate thermal conduction in amorphous silicon. *Phys. Rev. B* **97**, 024201 (2018).
21. Moon, J. et al. Thermal acoustic excitations with atomic-scale wavelengths in amorphous silicon. *Phys. Rev. Mater.* **3**, 065601 (2019).
22. Larkin, J. M., Turney, J. E., Massicotte, A. D., Amon, C. H. & McGaughey, A. J. Comparison and evaluation of spectral energy methods for predicting phonon properties. *J. Comput. Theor. Nanosci.* **11**, 249–256 (2014).
23. Kim, T., Moon, J. & Minnich, A. J. Origin of micrometer-scale propagation lengths of heat-carrying acoustic excitations in amorphous silicon. *Phys. Rev. Mater.* **5**, 65602 (2021).
24. Shenogin, S., Bodapati, A., Keblinski, P. & McGaughey, A. J. Predicting the thermal conductivity of inorganic and polymeric glasses: The role of anharmonicity. *J. Appl. Phys.* **105**, 034906 (2009).
25. Park, M., Lee, I. H. & Kim, Y. S. Lattice thermal conductivity of crystalline and amorphous silicon with and without isotopic effects from the ballistic to diffusive thermal transport regime. *J. Appl. Phys.* **116**, 043514 (2014).
26. Sääskilahti, K., Oksanen, J., Tulkki, J., McGaughey, A. J. & Volz, S. Vibrational mean free paths and thermal conductivity of amorphous silicon from non-equilibrium molecular dynamics simulations. *AIP Adv.* **6**, 121904 (2016).
27. Zhou, Y. Assessing the quantum effect in classical thermal conductivity of amorphous silicon. *J. Appl. Phys.* **129**, 235104 (2021).
28. Zhang, Z. et al. Heat conduction theory including phonon coherence. *Phys. Rev. Lett.* **128**, 015901 (2022).
29. Boon, J. P. & Yip, S. *Molecular Hydrodynamics* (Courier Corporation, 1991).
30. Moon, J. Examining normal modes as fundamental heat carriers in amorphous solids: the case of amorphous silicon. *J. Appl. Phys.* **130**, 055101 (2021).
31. Zhang, Z. et al. Generalized decay law for particlelike and wavelike thermal phonons. *Phys. Rev. B* **103**, 184307 (2021).
32. Xie, G., Ding, D. & Zhang, G. Phonon coherence and its effect on thermal conductivity of nanostructures. *Adv. Phys.: X* **3**, 1480417 (2018).
33. Gelin, S., Tanaka, H. & Lemaître, A. Anomalous phonon scattering and elastic correlations in amorphous solids. *Nat. Mater.* **15**, 1177–1183 (2016).
34. Zhou, Y. & Hu, M. Record low thermal conductivity of polycrystalline Si nanowire: breaking the casimir limit by severe suppression of propagons. *Nano Lett.* **16**, 6178–6187 (2016).

35. Zhou, Y., Morshedifard, A., Lee, J. & Abdolhosseini Qomi, M. J. The contribution of propagons and diffusons in heat transport through calcium-silicate-hydrates. *Appl. Phys. Lett.* **110**, 043104 (2017).
36. Beltukov, Y. M., Kozub, V. I. & Parshin, D. A. Ioffe-Regel criterion and diffusion of vibrations in random lattices. *Phys. Rev. B* **87**, 1–20 (2013).
37. Zhu, T. & Ertekin, E. Phonons, localization, and thermal conductivity of diamond nanothreads and amorphous graphene. *Nano Lett.* **16**, 4763–4772 (2016).
38. Seyf, H. R. & Henry, A. A method for distinguishing between propagons, diffusions, and locons. *J. Appl. Phys.* **120**, 025101 (2016).
39. Luckyanova, M. N. et al. Coherent phonon heat conduction in superlattices. *Science* **338**, 936–939 (2012).
40. Hu, S. et al. Randomness-induced phonon localization in graphene heat conduction. *J. Phys. Chem. Lett.* **9**, 3959–3968 (2018).
41. Hu, S. et al. Disorder limits the coherent phonon transport in two-dimensional phononic crystal structures. *Nanoscale* **11**, 11839–11846 (2019).
42. Zhang, Z. et al. Coherent thermal transport in nano-phononic crystals: an overview. *Sci. Rep.* **9**, 081102 (2021).
43. Ziman, J. M. *Electrons and Phonons: the Theory of Transport Phenomena in Solids* (Oxford University Press, 2001).
44. Zink, B. L., Pietri, R. & Hellman, F. Thermal conductivity and specific heat of thin-film amorphous silicon. *Phys. Rev. Lett.* **96**, 055902 (2006).
45. Gale, J. D. & Rohl, A. L. The general utility lattice program (GULP). *Mol. Simul.* **29**, 291–341 (2003).
46. Barbalinardo, G., Chen, Z., Lundgren, N. W. & Donadio, D. Efficient anharmonic lattice dynamics calculations of thermal transport in crystalline and disordered solids. *J. Appl. Phys.* **128**, 135104 (2020).
47. Zhao, Y. et al. Probing thermal transport across amorphous region embedded in a single crystalline silicon nanowire. *Sci. Rep.* **10**, 821 (2020).
48. Stokes, G. G. On the conduction of heat in crystals. *Math. Phys. Pap.* **5**, 203–227 (2010).
49. Zhang, Z., Hu, S., Chen, J. & Li, B. Hexagonal boron nitride: a promising substrate for graphene with high heat dissipation. *Nanotechnology* **28**, 225704 (2017).
50. Regner, K. T. et al. Broadband phonon mean free path contributions to thermal conductivity measured using frequency domain thermoreflectance. *Nat. Commun.* **4**, 1640 (2013).
51. Braun, J. L. et al. Size effects on the thermal conductivity of amorphous silicon thin films. *Phys. Rev. B* **93**, 140201(R) (2016).
52. Pan, Y., Zhou, J. & Chen, G. Quantifying thermal transport in amorphous silicon using mean free path spectroscopy. *Phys. Rev. B* **101**, 144203 (2020).
53. Plimpton, S. Fast parallel algorithms for short-range molecular dynamics. *J. Comput. Phys.* **117**, 1–19 (1995).
54. Stillinger, F. H. & Weber, T. A. Computer simulation of local order in condensed phases of silicon. *Phys. Rev. B* **31**, 5262–5271 (1985).
55. France-Lanord, A. et al. Atomistic amorphous/crystalline interface modelling for superlattices and core/shell nanowires. *J. Phys. Condens. Matter* **26**, 55011 (2014).
56. Schelling, P. K., Phillpot, S. R. & Keblinski, P. Phonon wave-packet dynamics at semiconductor interfaces by molecular-dynamics simulation. *Appl. Phys. Lett.* **80**, 2484–2486 (2002).
57. Jiang, P. et al. Total-transmission and total-reflection of individual phonons in phononic crystal nanostructures. *Sci. Rep.* **9**, 040703 (2021).

ACKNOWLEDGEMENTS

This work is partially supported by CREST JST (No. JPMJCR19I1 and JPMJCR19Q3). This research used the computational resources of the Oakforest-PACS supercomputer system, The University of Tokyo. This project is also supported in part by the grants from the National Natural Science Foundation of China (Grant Nos. 12075168 and 11890703), and Science and Technology Commission of Shanghai Municipality (Grant No. 19ZR1478600).

AUTHOR CONTRIBUTIONS

Z.Z.: methodology, investigation, writing. Y.G. and M.B.: discussion, writing—review and editing. J.C.: supervision, project administration, funding acquisition, writing—review and editing. M.N.: project administration, funding acquisition. S.V.: supervision, project administration, funding acquisition, writing—review and editing.

COMPETING INTERESTS

The authors declare no competing interests.

ADDITIONAL INFORMATION

Supplementary information The online version contains supplementary material available at https://doi.org/10.1038/s41524-022-00776-w.

Correspondence and requests for materials should be addressed to Zhongwei Zhang, Jie Chen or Sebastian Volz.

Reprints and permission information is available at http://www.nature.com/reprints

Publisher's note Springer Nature remains neutral with regard to jurisdictional claims in published maps and institutional affiliations.